A FLEXONIC MAGNETIC CAR FOR FERRO-STRUCTURAL HEALTH MONITORING

Jiajie Guo
School of Mechanical Engineering
Georgia Institute of Technology
Atlanta GA 30332-0405

Kok-Meng Lee
School of Mechanical Engineering
Georgia Institute of Technology
Atlanta GA 30332-0405

Dapeng Zhu
School of Civil and Environmental Engineering
Georgia Institute of Technology
Atlanta GA 30332-0355

Yang Wang
School of Civil and Environmental Engineering
Georgia Institute of Technology
Atlanta GA 30332-0355

ABSTRACT

This paper presents a new magnetic car as a mobile sensor node for health monitoring and dynamic testing of large civil (ferromagnetic) structures. Unlike traditional car design where the distance between the front and rear wheel pairs is fixed, the electromagnetically driven compliant beam (connecting the front and rear axles) not only offers an effective means to negotiate corners and cross ridges of small dimensions when maneuvering on ferromagnetic surfaces, but also serves as a sensor attachment device. Specifically, this paper presents the design concept of a novel flexonic magnetic car incorporating compliant beams and permanent magnets, and a three-dimensional model for simulating the deformed shape of the compliant beam. The compliant beam that enables direct contact of the accelerometer with the measuring surface eliminating the dynamic effect of the sensor carriers has been validated with the experimental modal analysis for a frame structure. This represents a transformative change from the fixed spatial resolution provided by traditional static sensors.

INTRODUCTION

Wireless sensor network has been widely developed in recent years for structural health monitoring of large civil structures subject to continuous static and dynamic loadings as well as environmental erosion. As a transformative change, the next revolution in sensor networks is predicted to be mobile sensor networks [1][2], in which each mobile sensing node can be an autonomous robot equipped with one or multiple smart sensors for exploring its surroundings and exchanging information with its peers through wireless communication.

In [3] the robot using ultrasonic motors for mobility and suction cups for adherence to crawl on a 2D surface was designed for visually inspecting aircraft exterior. A beam-crawler has been developed for wirelessly powering and interrogating battery-less peak-strain sensors; the crawler moves along the flange of an I-beam by wheels [4]. A twin-frame structure robot was developed to achieve both wheeled locomotion on flat ground and legged locomotion on uneven terrain [5]. Based upon magnetic on-off robotic attachment devices, a magnetic walker has been developed for maneuvering on a 2D surface [6]. In order to inspect carbon steel pipe, a magnetic wheeled robot has been developed to move automatically along the outside of piping [7]. Motivated by non-invasive surgery, a micro robot has been studied to run in human vessels or gastro-intestine system [8].

Due to the high complexity of large civil structural systems, the locations where damage occur can be largely unpredictable. A number of new damage identification technologies have been developed for infrastructure applications; most notably the vibration-based methods. Previous vibration-based damage identification methods for civil structures largely focus on global vibration characteristics. In order to closely monitor the structure, the cost and difficulty associated with dense arrays of wireless sensors are still prohibitive for wide deployment in practice. Mobile sensor networks offer flexible architectures, which lead to adaptable spatial resolutions that are unavailable from static wireless sensors. Unlike vibration analysis based upon global modal parameters of the entire structure, mobile sensors with excitation functionality can excite only a local area of the structure. Local excitation can offer high signal-to-noise ratios, and provide vibration data that are more sensitive to non-significant but developing damages. To be effective, sensors (such as accelerometers) on the mobile carriers must be in direct contact with the structure when performing

measurements so that high frequency components can be reliably measured for modal analyses.

Developing a new robot for a specific structure is always time consuming and monetary costly. It is beneficial to develop a general method to design robots that can move on different kinds of complex structures. For the above reasons, this paper presents the design concept and development of a flexure-based mechatronic (flexonic) car for maneuvering different kinds of obstacles on ferromagnetic surfaces. The wheels of the flexonic car are augmented with properly designed permanent magnets (PMs) that increase the normal force to overcome the effect of gravity. Because compliant mechanisms have no relative moving parts and thus no contact frictional dissipation, flexible structures have been studied on compliant robots; see for examples [9][10][11][12] where focuses have been on modeling and control. In this paper, the flexure-based architecture offers different poses (and thus higher degrees of freedom) to negotiate obstacles (including narrow sections and high abrupt angle changes) commonly encountered in complex civil structures.

The remainder of this paper offers the followings:

− We present the design concept of a novel magnetically driven flexonic car incorporating compliant beams and PMs. Apart from offering the ability to negotiate difficult obstacles, the compliant beam offers an effective means to attach or detach a sensor (on or from the surface of the structure) for making measurement.

− A general quasi-static compliant beam model for simulating 3D beam deformation is offered to serve as an essential basis for design/control of a flexonic car as mobile sensor node for applications such as structural health monitoring.

− Three sets of results provide insights to the compliant beam deformation for magnetic car applications. The 1st illustrates the effect of the (front-to-rear) wheel distance on negotiating a corner. The 2nd illustrates numerically the loading conditions to achieve the desired bending and/or twisting of a compliant beam. As demonstrated in the 3rd set of FFT results, the compliant beam enables direct contact of the accelerometer with the measuring surface eliminating the dynamic effect of the sensor carriers.

DESIGN CONCEPT OF A FLEXONIC MOBILE NODE

Figure 1(a) shows the prototype flexonic magnetic mobile sensor node capable of moving and attaching (or detaching) a sensor on (or from) ferromagnetic structures. The mobile node consists of two pairs of magnetic wheels (each driven by an electric motor), microprocessor PWM control, and wireless communication and associated hardware circuits. The mobile node, sensor and four 9V rechargeable batteries are mounted on a flexible structure (manufactured from one piece of Delrin material) as shown in Fig. 1(b). The overall weight of the mobile sensor node is 1kg, most of which is contributed by the magnet wheels, electric motors and batteries. As shown in Fig. 1(b), the compliant beam (connecting the magnetic wheel-pairs) serves two functions.

The *first* function is to attach/detach an accelerometer (mounted on a platform in the middle of the flexible beam) on/from the surface to be measured as shown in Fig. 2. When a measurement is to be made, the two wheel-pairs are driven away from each other straightening the compliant beam as shown in Fig. 2(a) allowing the accelerometer (not shown) to be pressed against the surface to be measured. During the car-moving operation, the compliant beam is normally buckled upward and held in position under the attraction between a pair of fixed iron bars and a pair of magnets on both sides of the sensor holder. The buckling of the beam frees the accelerometer from the surface as shown in Fig. 2 (b).

(a) Prototype   (b) CAD Model
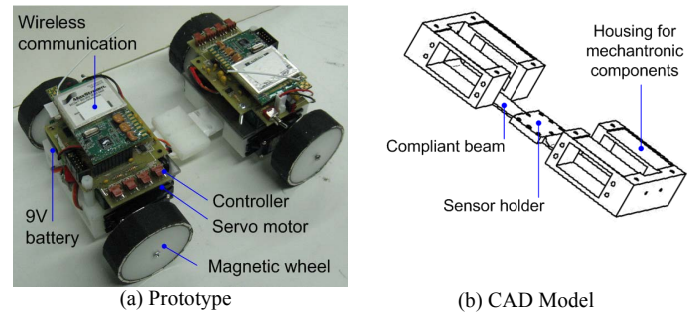
FIGURE 1. FLEXONIC MAGNET WHEEELED CAR

(a) Not buckled   (b) buckled
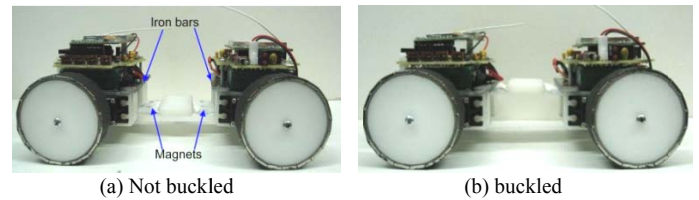
FIGURE 2. THE COMPLIANT BEAM BUCKLING

The *second* function is to provide a means to overcome obstacles when navigating on a structure. Among the challenging obstacles is the crossing of a reinforcing ridge of small dimensions. As illustrated in Fig. 3, the magnetic wheel must negotiate sharp corners. Magnetic forces at the corner greatly decrease when negotiating a concave corner, but increase (because of multiple contacts) when moving up or down a convex corner. Unlike a traditional design with a fixed distance between the front and rear wheels, the compliant beam of the flexonic magnetic car can be shortened by buckling and thus can be designed to offer additional contact forces as needed by bending the connecting beam. Other challenges include a change in direction onto different surfaces as shown in Figs. 4 and 5, which require the compliant beam to twist in addition to bending. The ability to combine twist and bend enables the car to change directions across multiple orthogonal planes. Figure 5 shows an example where the car moves from the 1st plane by bending to the 2nd plane, and immediately to the 3rd plane by twisting since the 2nd plane is too narrow to accommodate the whole car.

The functions illustrated in Figs. 3 to 5 require an appropriate loading specification to realize the bending and/or twisting in addition to the boundary conditions in formulating a compliant beam model to be discussed in the next section.

(a) reinforced ridge   (b) concave corner   (c) convex corner   (c) crossing a ridge
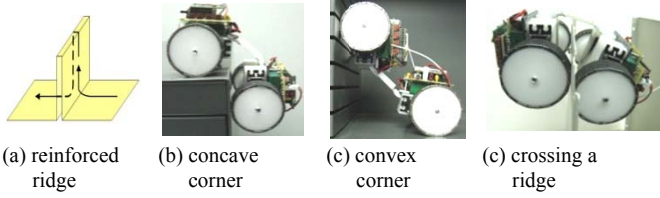
FIGURE 3 COMPLIANT BEAM BENDING
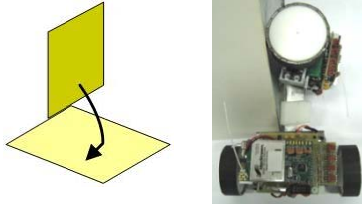
FIGURE 4. TWISTING FOR A 90° DIRECTION CHANGE
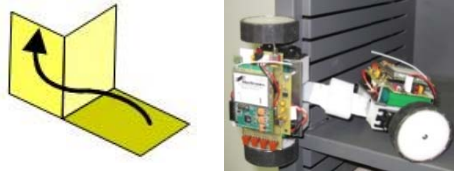
FIGURE 5. TWIST/BEND FOR DIRECTION CHANGE ON DIFFERENT SURFACES

QUASI-STATIC MODEL OF A 3D COMPLIANT BEAM

Figure 6 shows a compliant beam model. The initial curved shape is described by (1):

$$\frac{d}{ds}\begin{bmatrix}\mathbf{i}_x & \mathbf{i}_y & \mathbf{i}_z\end{bmatrix}^\mathrm{T} = \mathbf{k}\times\begin{bmatrix}\mathbf{i}_x & \mathbf{i}_y & \mathbf{i}_z\end{bmatrix}^\mathrm{T} \tag{1}$$

where the unit vectors $\mathbf{i}_x$, $\mathbf{i}_y$ and $\mathbf{i}_z$ are along the axes x, y and z; and $\mathbf{i}_1$, $\mathbf{i}_2$ and $\mathbf{i}_3$ along the axes ξ, η and ζ; s is the undeformed arc length from the root of the beam to the reference point on the observed cross-section; and $\mathbf{k} = [k_1, k_2, k_3]^\mathrm{T}$ describes the initial curvatures.

The deformed and un-deformed coordinate systems are related by a rotational matrix $[\mathbf{T}]$:

$$\begin{bmatrix}\mathbf{i}_1 & \mathbf{i}_2 & \mathbf{i}_3\end{bmatrix}^\mathrm{T} = [\mathbf{T}][\mathbf{i}_x \quad \mathbf{i}_y \quad \mathbf{i}_z]^\mathrm{T} \tag{2}$$

where $[\mathbf{T}]^\mathrm{T} = [\mathbf{T}_1 \quad \mathbf{T}_2 \quad \mathbf{T}_3]$; and $\mathbf{T}_i = [T_{i1} \quad T_{i2} \quad T_{i3}]^\mathrm{T}$. Because of the orthogonal property $[\mathbf{T}]^\mathrm{T} = [\mathbf{T}]^{-1}$, $[\mathbf{T}]$ can be written as

$$[\mathbf{T}] = \begin{bmatrix}1 & 0 & 0 \\ 0 & \cos\varphi & \sin\varphi \\ 0 & -\sin\varphi & \cos\varphi\end{bmatrix}[\mathbf{B}(\alpha)] \tag{3}$$

where φ is an Euler angle for twisting about the ξ axis; and the transformation matrix $[\mathbf{B}(\alpha)]$ is due to the bending rotation α as shown in Fig. 6. In (2),

$$\cos\alpha = T_{11} = \mathbf{i}_1\bullet\mathbf{i}_x; \quad \sin\alpha = |\mathbf{i}_1\times\mathbf{i}_x| = \sqrt{T_{12}^2 + T_{13}^2}. \tag{4a,b}$$

For $0° \le \alpha < 180°$ ($T_{11} \ne -1$), $[\mathbf{B}(\alpha)]$ is given in terms of $\mathbf{T}_1$ and φ in (12) [13][14]:

$$[\mathbf{B}(\alpha)] = \begin{bmatrix} T_{11} & T_{12} & T_{13} \\ -T_{12} & T_{11}+T_{13}^2/(1+T_{11}) & -T_{12}T_{13}/(1+T_{11}) \\ -T_{13} & -T_{12}T_{13}/(1+T_{11}) & T_{11}+T_{12}^2/(1+T_{11}) \end{bmatrix} \tag{5}$$

Since $\quad \|\mathbf{T}_1\| = T_{11}^2 + T_{12}^2 + T_{13}^2 = 1 \tag{6}$

3 of the 4 variables (T_{11}, T_{12}, T_{13}, φ) in $[\mathbf{T}]$ are independent.
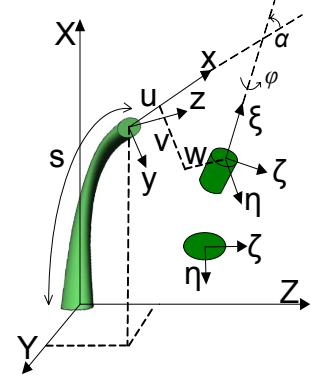
FIGURE 6. A COMPLIANT BEAM

For negligible torsional warping, the axial strain e and the curvatures after deformation $\boldsymbol{\rho}=[\rho_1, \rho_2, \rho_3]^\mathrm{T}$ can be expressed using the following relationship [14]:

$$\begin{bmatrix}e \\ \boldsymbol{\rho}\end{bmatrix} = diag\left[\frac{1}{EA}, \frac{1}{GJ}, \frac{1}{EI_{22}}, \frac{1}{EI_{33}}\right]\begin{bmatrix}F_1 \\ \mathbf{M}\end{bmatrix} + \begin{bmatrix}0 \\ \mathbf{k}\end{bmatrix} \tag{7}$$

where E is the elastic modulus; G is the shear modulus; A is the cross section area; J is the polar moment of inertia; and I_{22} and I_{33} are the moments of inertia.

The force and moment equations for the 3D compliant beam are given by (8a) and (8b) respectively:

$$\mathbf{F}' = -\boldsymbol{\rho}\times\mathbf{F} - [\mathbf{T}]\mathbf{q}_F \tag{8a}$$

$$\mathbf{M}' = -\boldsymbol{\rho}\times\mathbf{M} - (1+e)\begin{bmatrix}0 & -F_3 & F_2\end{bmatrix}^\mathrm{T} - \mathbf{q}_M \tag{8b}$$

where $\mathbf{F}=[F_1, F_2, F_3]^\mathrm{T}$ and $\mathbf{M}=[M_1, M_2, M_3]^\mathrm{T}$ are the force and moment in $\xi\eta\zeta$ coordinates respectively; the derivatives (denoted by $'$) is taken with respect to the path length s; $\mathbf{q}_F$ are distributed forces acting along the axes x, y and z; and $\mathbf{q}_M$ are the distributed moments acting along the axes ξ, η and ζ. From (11) to (5), we have

$$\mathbf{T}_1' = \rho_3\mathbf{T}_2 - \rho_2\mathbf{T}_3 - \mathbf{k}\times\mathbf{T}_1 \tag{8c}$$

$$\begin{bmatrix}1+u' & v' & w'\end{bmatrix}^\mathrm{T} = \mathbf{k}\times\begin{bmatrix}u & v & w\end{bmatrix}^\mathrm{T} + (1+e)\mathbf{T}_1 \tag{8d}$$

$$\varphi' = \rho_1 - \mathbf{k}\bullet\mathbf{T}_1 - (T_{13}T_{12}' - T_{12}T_{13}')/(1+T_{11}) \tag{8e}$$

where u, v and w are the displacements of the observed reference point in the directions of axes x, y and z respectively.

The four vector and one scalar equations, (8a-e), are the 13 governing equations for solving the 13 unknowns (F_1, F_2,

F_3; M_1, M_2, M_3; T_{11}, T_{12} T_{13}; u, v, w; φ); 12 of them are independent. The boundary condition problem (BVP) characterized by (8) can be recast as an initial value problem (IVP) for solving by a multiple shooting method [15] in Appendix at the end of this paper.

RESULTS

Results are obtained to investigate the effects of key design optimal parameters on the ability to negotiate obstacles, and to investigate the effect of sensor attachment on modal analysis.

Wheel kinematics for right-angle corners

Unlike a traditional design that has a fixed distance between the front and rear axles, the compliant beam between axles offers a significant advantage in negotiating the corner. Without loss of generality we assume non-slip rolling and both the front and rear wheels rotate at a constant speed in the following discussion. As an illustration, Figs. 7 and 8 plot the normalized wheel spacing d_1/r and the normalized distance d_2/r when negotiating a right-angle corner, where r is the wheel radius; d_1 is the distance between front and rear wheel axles; and d_2 is the distance from the non-deflected beam to the corner.
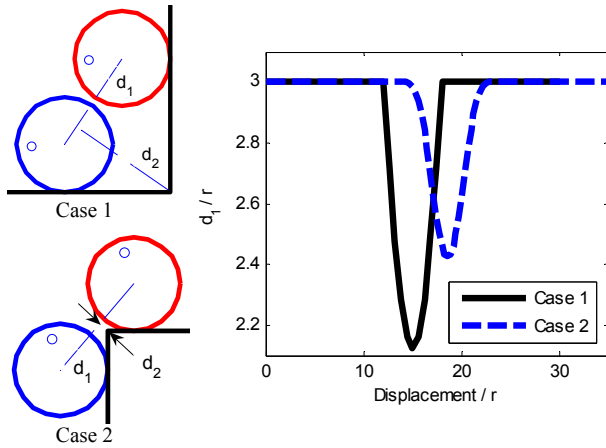
FIGURE 7. DISTANCES BETWEEN WHEELS
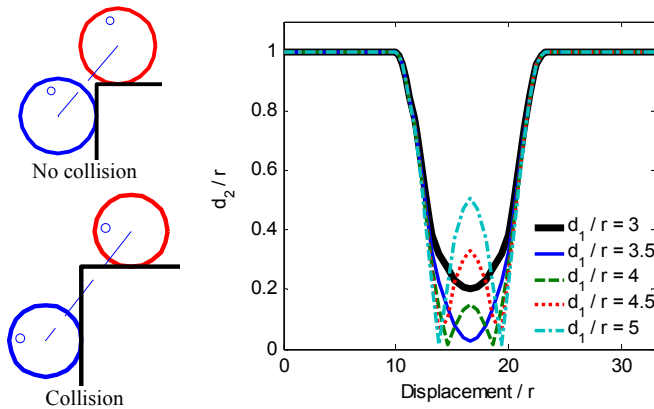
FIGURE 8. DISTANCE BETWEEN CORNER AND BEAM

Some general observations can be made from the results:
− Fig. 7 shows that d_1/r shortens when negotiating a right-angle corner. This suggests that the compliant beam can be appropriately design for buckling to negotiate a corner.
− Collision avoidance is designed on Case 2. As shown in Fig. 8, d_1/r should be no more than 3.5.

Compliant beam analysis

In order to negotiate commonly encountered obstacles, the loading condition on a compliant beam must be appropriately specified. As an illustration, the three different poses in Figs. 3, 4 and 5 (under bending, twisting and their combination respectively) are numerically simulated. The dimension, material properties and boundary conditions used in simulating the compliant beam are given in Table 1.

TABLE 1. PARAMETERS AND BOUNDARY CONDITIONS

Beam geometry		Material properties	
Length (cm)	6.6	Elastic Modulus (GPa)	3.1
Width (cm)	2.2	Shear Modulus (Gpa)	1.15
Thickness (mm)	1.3	Poisson ratio	0.35
		Density (kg/m^3)	1.42
Boundary conditions			
$s = 0$: $T_{11} = 1$, $T_{12} = 0$, $T_{13} = 0$, $\varphi = 0$, $u = v = w = 0$;			
$s = L$: $F_x = 0$, $F_y = 0$, $F_z = F$, $M_x = M$, $M_y = 0$, $M_z = 0$;			
Bending		$F = 14.15$N, $M = 0$	
Twisting		$F = 0$, $M = 0.238$N·m	
Bending & Twisting		$F = 14.15$N, $M = 0.238$N·m	

Since the beam is symmetric, only one front-half of the beam is simulated. In addition, the sensor holder is much thicker (and hence much more rigid) than the compliant beam, only the section between the fixed end to the sensor holder is considered as the compliant beam discussed here. The effects of three different loading conditions of the compliant beam are illustrated in Fig. 9.

− When the car negotiates a corner or crossing a ridge (Fig. 3), the connecting beam can be bent by exerting horizontal forces provided by the wheels as shown in Fig. 9(a).
− When the car goes through a curve path which requires the compliant beam to twist (Fig. 4), the deformed shape can be obtained by exerting a pure moment along the longitudinal axis as illustrated in Fig. 9(b).
− A more general loading which results in a combination of bending and twisting is illustrated in Fig. 9(c) for application where the magnetic car must cross multiple planes to avoid narrow structure (Fig. 5).

Modal analysis

In [16], modal analysis of a frame structure (similar to Fig. 10) was conducted with data collected from four mobile sensing nodes, where sensors were not in contact with the measuring surface. The modal analysis in [16] was limited to

50Hz due to the car dynamics of the mobile sensing node which essentially behaves as a low-pass filter. The interest here is to investigate the effect of sensor attachment on the modal analysis using impulse response studies. For this, vertical vibration data were obtained from both the 4-wheel magnetically driven flexonic car with a compliant beam, and the 3-wheel magnetic car [16][17] where the accelerometer (underneath the car) is not in contact with the surface. The accelerometer of the flexonic car is firmly pressed against the measured surface by the compliant beam and magnets as compared in Fig. 11. As a basis for comparison, the FFT results obtained from both measurements are compared against those predicted by finite element method (FEM).

(a) Bending

(b) Twisting

(c) Combined bending and twisting
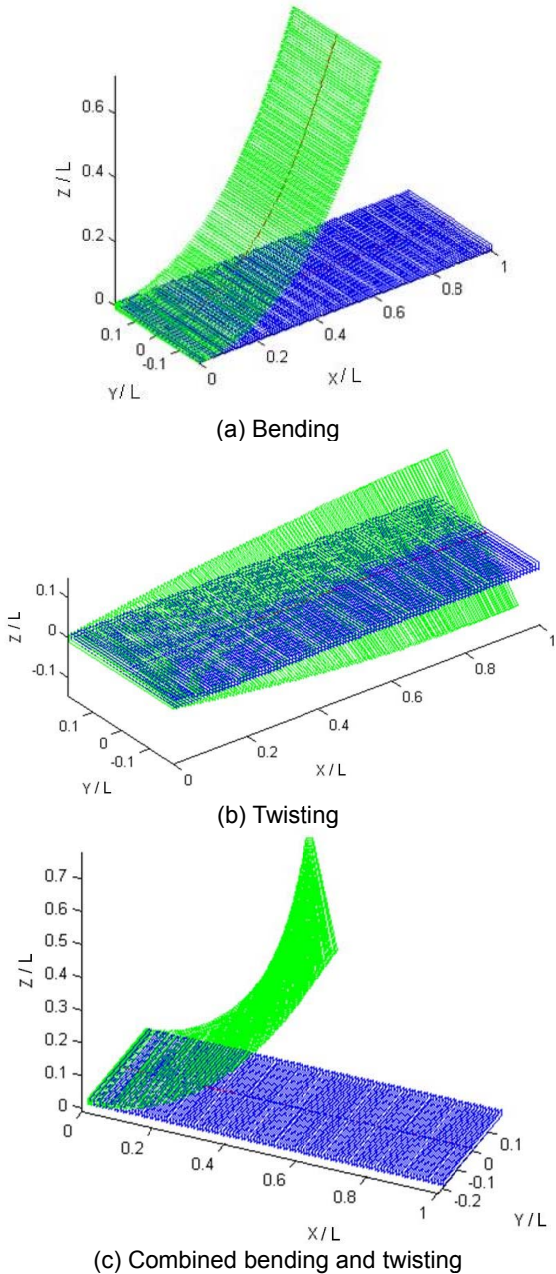
FIGURE 9. A COMPLIANT BEAM DEFORMATION

Figure 10 shows a 2D laboratory steel portal frame structure (consisting of a beam and two column members) constructed for structural modal analyses. The beam is connected to the columns by bolted angle plates, and by hinge-connections at the column bases, Material properties for the frame structure are listed in Table 2 along with the dimensions in Fig. 10. The two mobile cars are placed at the same position on the beam where vertical vibration data were collected after a hammer impact at a specified position. A sampling frequency of 500Hz is used for the data collection. The results comparing the vertical vibration data (in frequency domain) collected from the two cars are given in Fig. 12 and Table 3.
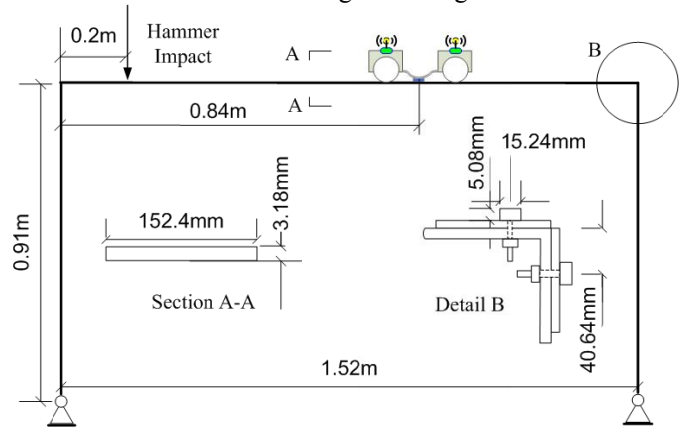
FIGURE 10. STEEL FRAME STRUCTURE
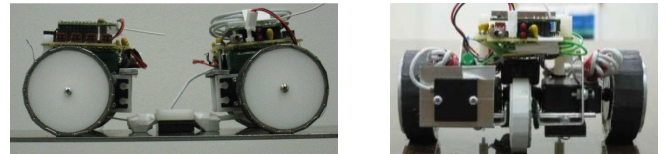
(a) Flexonic   (b) Single axle [16]

FIGURE 11. TWO DESIGNS OF MAGNETIC CARS

TABLE 2. MATERIAL PROPERTIES FOR STRUCTURE

Material properties	Steel	Car dimensions	
Elastic Modulus (GPa)	210	Length (cm)	20
Shear Modulus (GPa)	82	Width (cm)	14.7
Poisson ratio	0.28	Height (cm)	7.6
Density (kg/m^3)	7700	Weight (kg)	1
Sampling frequency = 500 Hz			

Some observations can be made from the results:

− The dynamics of both magnetic cars has little influence on the lower-frequency (<50Hz) vibration measurements, and thus the results are closely matched with FEM results.

− For this experiment configuration, the 1st vibration mode (horizontal) is not excited, so the lowest modal frequency is not identified. Also, since only one measuring point is considered in the experiment, some of the modal frequencies obtained from FEM are not detected. Clearly, if this measuring point is at the zeros of certain modal shapes,

the corresponding frequencies for these modal shapes cannot be captured at this point suggesting that multiple measuring points are necessary in practice.

− For frequencies larger than 50Hz, relatively sharp peaks can

still be identified by the flexonic magnetic car (with a compliant beam) because the accelerometer is firmly pressed against the steel frame structure eliminating the car dynamic effects on the measurements.
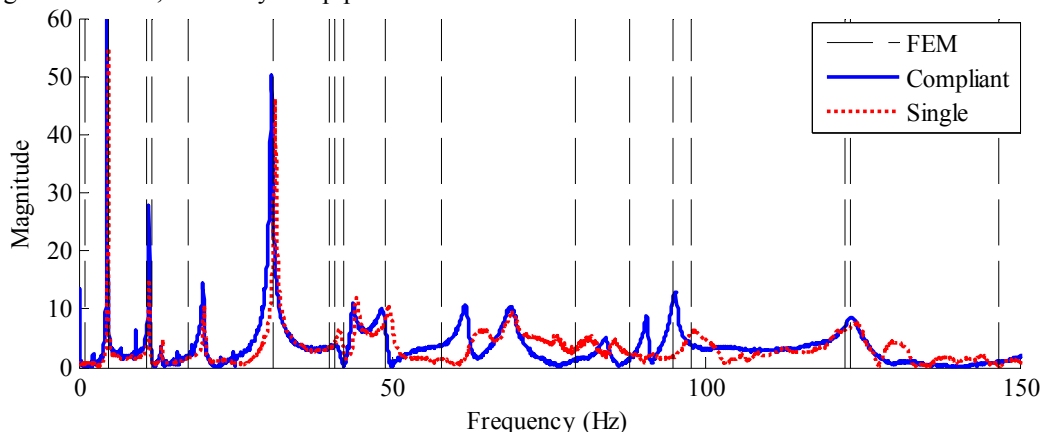
FIGURE 12. FFT OF VERTICAL VIBRATION

TABLE 3. COMPARISON OF FREQUENCIES

FEM (Hz)	Compliant (Hz)	Single (Hz)
1.009		
4.626	4.5	4.7
10.757		
11.642	11.2	11.2
17.573	19.9	20.1
30.970	30.8	31.3
39.946		
40.679	43.8	44.3
42.247		
48.816	48.3	49.5
57.758	61.8	
79.232		
87.724	90.5	
94.619	95.1	98.2
97.680		
122.150	123.3	124.2
123.130		
146.640		

CONCLUSION

Along with an analytical model for simulating the deformed shape of a compliant beam in 3D space, a flexonic magnetic car incorporating a compliant mechanism has been designed to carry sensors for placing on a ferromagnetic structure. Several examples were simulated to illustrate the specified loading for bending and/or twisting the compliant beam to negotiate obstacles. These studies include a kinematics analysis which investigates the effect of the wheel distance on collision avoidance when crossing a corner. The analysis suggests that when the beam is buckled, the wheel distance-radius ratio should be less than 3.5. The exploratory

study on a prototype car, which is also independently supported by a quasi-static flexible beam analysis, demonstrates the feasibility of several obstacle-crossing strategies, so further investigation in control design and resulting dynamics analysis is worth of exploration. Finally, the experimental modal analysis on a frame structure shows that the flexonic magnetic car (that enables direct contact of the accelerometer with the measuring surface) has the ability to eliminate the dynamic effect of the sensor carriers, which represents a transformative change from the fixed spatial resolution provided by traditional static sensors.

REFERENCES
[1] Akyildiz, I.F., Su, W. Sankarasubramaniam, Y. and Cayirci, E., 2002, "A survey on sensor networks," *IEEE Commun. Mag.*, 40(8), pp.102-144.

[2] LaMarca, A., Brunette, W., Koizumi, D., Lease, M., Sigurdsson, S.B., Sikorski, K., Fox, D. and Borriello, G., 2002, "Making sensor networks practical with robots," Proceedings of the First International Conference on Pervasive Computing, pp.152-166, Zurich, Switzerland.

[3] Backes, P.G., Bar-Cohen, Y. and Joffe, B., 1997, "The multifunction automated crawling system (MACS)," *Proceedings of the 1997 IEEE International Conference on Robotics and Automation*, 1: 335-340, Albuquerque, New Mexico.

[4] Huston, D.R., Esser, B., Gaida, G., Arms, S.W. and Townsend, C.P., 2001, "Wireless inspection of structures

aided by robots," *Proceedings of SPIE, Health Monitoring and Management of Civil Infrastructure Systems*, 4337: 147-154, Newport Beach, CA.

[5] Ota, Y., Yoneda, K., Tamaki, T., Hirose, S., 2002, "A walking and wheeled hybrid locomotion with twin-frame structure robot," *IEEE/RSJ International Conference on Intelligent Robots and System*, Volume 3, 30 Sept.-5 Oct. pp.2645 – 2651.

[6] Brian, E., Jon, M., Dryver, R.H. and Phil, B., 2004, "Robotic systems for homeland security," *Proceedings of SPIE, Nondestructive Detection and Measurement for Homeland Security II*, 5395: 134-142, San Diego, CA.

[7] Yukawa, T., Suzuki, M., Satoh, Y., Okano, H., 2006, **"**Design of Magnetic Wheels in Pipe Inspection Robot", IEEE International Conference on Systems, Man and Cybernetics, 8-11 Oct. pp: 235 – 240.

[8] He, B., Lu, P., Yue, J., Zhou, Y., 2006, "Study on a Novel Kind of Micro Robot for Non-Invasive Surgery," The Sixth World Congress on Intelligent Control and Automation, WCICA, Volume 2, pp. 9134 – 9138.

[9] Ahmad, S., 1993, "Control of cooperative multiple flexible joint robots," *IEEE Transactions on Systems, Man and Cybernetics*, 23(3), May-June, pp. 833 – 839.

[10] Arteaga, M.A., Siciliano, B., 2000, "On tracking control of flexible robot arms," IEEE Transactions on Automatic Control, 45(3), March , pp.520 – 527.

[11] Filipovic, M., Vukobratovic, M., 2005, **"**Modeling of Flexible Robotic Systems", *The International Conference on Computer as a Tool, EUROCON*, Volume 2, 21-24 Nov. pp.1196 - 1199 .

[12] Garcia, J.G., Robertsson, A., Ortega, J.G., Johansson, R., 2008, "Sensor Fusion for Compliant Robot Motion Control**,"** IEEE Transactions on Robotics, 24(2) April pp.430 – 441.

[13] Alkire, K., 1984, *An analysis of rotor blade twist variables associated with different Euler sequences and pretwist treatments*. NASA TM 84394.

[14] Pai, P.F., Palazotto, A.N., 1996, "Large-deformation analysis of flexible beams," *International Journal of Solids Structures*, 33(9), pp. 1335-1353.

[15] Stoer, J., Bulirsch, R., 1980, *Introduction to Numerical Analysis*, 2nd, pp. 476-477, Springer-Verlag, New York.

[16] Zhu D., Q. Qi, Y. Wang, K.-M. Lee, and S. Foong, 2009, "A prototype mobile wireless sensor network for structural health monitoring," in *Proceedings of SPIE, Nondestructive Characterization for Composite Materials, Aerospace Engineering, Civil Infrastructure, and Homeland Security*, San Diego, CA, 8–12 March, pp. 72941A-1 to 72941A-10.

[17] Lee K.-M., Wang Y., Zhu D., Guo J. and Yi X., 2009, "Flexure-based mechatronic mobile sensors for structure damage detection," *Proceedings of the 7th International Workshop on Structural Health Monitoring*, Stanford, CA, September 9 - 11.

ANNEX A

MULTIPLE SHOOTING METHOD (MSM)

The boundary condition problem (BVP) of a 3D compliant beam can be written in the following form:

$$\mathbf{X}' = \mathbf{f}(s, \mathbf{X}), \quad \mathbf{g}(\mathbf{X}(0), \mathbf{X}(L)) = \mathbf{0} \qquad (A.1)$$

where $\mathbf{X}$ is a vector of the 13 variables; $0 \leq s \leq L$ with L being the beam length; and $\mathbf{g}(\bullet)$ is the boundary conditions (BCs) specifying the geometrical loading constraints at both ends. The BVP (A.1) is recast as an initial value problem (IVP) and solved using a MSM [15]. For this, the region $[0, L]$ is divided into $m\text{-}1$ sections by m nodes as shown in Fig. A, where s_i is the arc length from the root of the beam to the ith node; $x_i^{(n)}$ is the initial guesses for the ith section, and the superscript (n) denotes the nth guess.
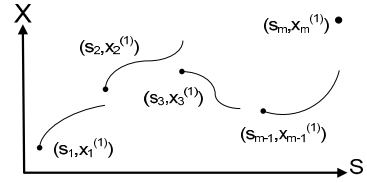
Fig. A. Multiple shooting method

The BVP can then be posed as a set of m 1st-order non-linear equations (A.2) subject to a set of m constraints (A.3) as functions of the initial guesses:

$$\mathbf{X}' = \mathbf{f}(s, \mathbf{X}), \quad \mathbf{X}(s_i) = \mathbf{x}_i^{(n)} \qquad (A.2)$$

$$\mathbf{C}(\mathbf{x}^{(n)}) := \begin{bmatrix} \mathbf{C}_1(\mathbf{x}_1^{(n)}, \mathbf{x}_2^{(n)}) \\ \vdots \\ \mathbf{C}_{m-1}(\mathbf{x}_{m-1}^{(n)}, \mathbf{x}_m^{(n)}) \\ \mathbf{C}_m(\mathbf{x}_1^{(n)}, \mathbf{x}_m^{(n)}) \end{bmatrix} := \begin{bmatrix} \mathbf{X}(s_2; s_1, \mathbf{x}_1^{(n)}) - \mathbf{x}_2^{(n)} \\ \vdots \\ \mathbf{X}(s_m; s_{m-1}, \mathbf{x}_{m-1}^{(n)}) - \mathbf{x}_m^{(n)} \\ \mathbf{g}(\mathbf{x}_1^{(n)}, \mathbf{x}_m^{(n)}) \end{bmatrix} \qquad (A.3)$$

Using Newton method, the initial guesses are updated using (A.4):

$$\mathbf{x}^{(n+1)} = \mathbf{x}^{(n)} - \alpha \left[D\mathbf{C}(\mathbf{x}^{(n)}) \right]^{-1} \mathbf{C}(\mathbf{x}^{(n)}), \quad n = 0,1,\dots \qquad (A.4)$$

where $D\mathbf{C} = \partial\mathbf{C}/\partial\mathbf{x}^{(n)}$ is a matrix, α is a coefficient for the iteration step size. The iteration process of (A.4) stops until $\mathbf{C}(\mathbf{x}^{(n)}) \rightarrow \mathbf{0}$ (or a small tolerance error Err_{tol}) implying that the solution is continuous and satisfies the BCs.   The MSM can be implemented using the following steps:

1. Set the initial guess $\mathbf{x}^{(0)} = [\mathbf{x}_1^{(0)} \quad \mathbf{x}_2^{(0)} \quad \cdots \quad \mathbf{x}_m^{(0)}]$.
2. Solve the IVP (9a) with $\mathbf{X}(0) = \mathbf{x}^{(0)}$.
3. Calculate the residual $\|\mathbf{C}(\mathbf{x}^{(0)})\|$ and corresponding $D\mathbf{C} = \partial\mathbf{C}/\partial\mathbf{x}^{(0)}$.
4. Update the initial guess by (A.4).
5. Repeat steps 2~4 (replacing $x^{(0)}$ with $x^{(n)}$) until $\|C(x^{(n)})\| <$ tolerance error Err_{tol}.